

# Hybrid Multi-Sensor Navigation System with Uncertainty Correction for GNSS-Denied Environments

Mar Villalonga Torres<sup>1</sup>, Tarafder Elmi Tabassum<sup>2</sup>, Dr Ivan Petrunin<sup>3</sup>  
and Prof Antonios Tsourdos<sup>4</sup>

*Cranfield University, Bedford, MK43 0AL, United Kingdom*

**Acknowledging the vulnerabilities of the Global Navigation Satellite Systems (GNSS) to various interferences, this research investigates alternative navigation solutions, essential for overcoming challenges where GNSS quality is compromised. The study explores a multi-sensor solution, suitable for operation in complex scenarios including degraded environmental conditions. To mitigate the inherent drifting behavior of a widely used alternative navigation information source referred to as the Inertial Navigation System (INS), fusion with a camera and a barometer is adopted within the federated multi-sensor architecture. This approach utilizes an error detection mechanism based on analysis of residual test statistics for Extended Kalman Filter (EKF)-based local filters. To enhance the robustness of the system, a Bidirectional Long Short-Term Memory (BiLSTM) model is implemented for error correction of the filter measurements, integrated before fusion in the master filter. Validation tests in a simulated urban environment using various trajectories and environmental conditions reveal that the proposed mechanism provides a viable alternative to a GNSS-based system for positioning. The performance is compared with the state-of-the-art learning-based multi-sensor navigation system by testing on similar datasets. Comparative results indicate significant improvements in positioning with error correction yielding enhancements of 34%, 44%, and 20% in rainy, snowy and foggy conditions, respectively.**

## I. Nomenclature

$\hat{\mathbf{x}}_{k k}$	=	Estimated state
$P_{k k}$	=	Measurement covariance matrix
$\mathbf{v}_k$	=	Residual vector
$K_k$	=	Kalman gain
$Q_k$	=	Process noise covariance matrix
$R_k$	=	Measurement noise covariance matrix
$\lambda_x, \lambda_y$	=	Estimated scale factor at $x$ and $y$ axis
$W_s^i$	=	Weighted samples
$\mathbf{\varepsilon}_{1k}, \mathbf{\varepsilon}_{2k}$	=	Predicted position increments
$\chi^*$	=	Test statistics
$M$	=	Number of training samples
$Z_k$	=	Measurement vector
$S_k$	=	Variance of residual values

<sup>1</sup> MSc Student, School of Aerospace, Manufacturing and Transport, Cranfield University, Bedford, MK43 0AL, United Kingdom.

<sup>2</sup> PhD Researcher, School of Aerospace, Manufacturing and Transport, Cranfield University, Bedford, MK43 0AL, United Kingdom.

<sup>3</sup> Reader, School of Aerospace, Manufacturing and Transport, Cranfield University, Bedford, MK43 0AL, United Kingdom.

<sup>4</sup> Professor, Head of the Centre of Autonomous and Cyber-Physical Systems, School of Aerospace, Manufacturing and Transport, Cranfield University, Bedford, MK43 0AL, United Kingdom.

## II. Introduction

In the past decades, Global Navigation Satellite Systems (GNSS) has become a primary option for navigation in most Unmanned Aerial System (UAS) applications due to its ability to provide highly accurate Position, Navigation, and Timing (PNT) information. However, the inherent reliance of GNSS-based systems on weak satellite signals renders these systems susceptible to various forms of interference including jamming, spoofing, multipath, non-line-of-sight reception and atmospheric effects. To address such challenges, a common approach involves integrating GNSS with other measurements from aiding sensors or systems, such as an Inertial Navigation System (INS). However, this fusion cannot fully address all integrity concerns. The main limitations lie in the cumulative degradation of accuracy over time due to errors in inertial sensors for integral computations [3]. With advances in UAS technologies, and their wider and more demanding applications, the limitations of GNSS-based navigation in challenging environments accentuate the critical need to explore alternative navigation solutions. Such alternatives ought to guarantee end-to-end safety of navigation while also ensuring integrity monitoring capabilities. Certainly, the application of alternative navigation in GNSS-denied environments requires enabling a high level of safety and reliability. Recently, UAS navigation in GNSS-denied environments has attracted significant attention, with a particular emphasis on integrating visual and inertial sensor information, referred to as Visual Inertial Odometry (VIO). The fusion strategies proposed by state-of-the-art VIO systems are not performing well when VIO suffers from degradation factors including moving objects, illumination changes, noise measurements, weather effects, and texture-less environments [1]–[4]. Furthermore, the majority of the studies exploring the integration of GNSS/INS/VO in GNSS-denied environments focus on improving GNSS and INS measurements, whilst navigation performance strongly relies on visual information extracted from the environment. Thus, there is still a research gap in developing error correction solutions with consideration of all the sensors contributing to alternative GNSS within a multi-sensor navigation system.

This work contributes towards addressing this problem by proposing and exploring the multi-sensor navigation system for UAS integrating GNSS, INS, VO, and barometer within a federated architecture. It explores the system performance under conditions when GNSS is only available at the take-off, compensating also the vulnerability of the visual-inertial odometry to the quality of the input features and complexity of the measurement corrections by application of a recurrent learning algorithm - Bidirectional Long Short-Term Memory (BiLSTM) that has been employed as the error corrector for the local filter outputs. Furthermore, the study also addresses the challenges of Visual Odometry (VO) when operating at high altitudes since monocular VO provides only 2D positioning. To compensate for VO's potential errors in vertical positioning, the barometer, serving as an altimeter is incorporated within the navigation system.

The remainder of the paper is organized as follows. Section 3 summarizes related works. Section 4 introduces the proposed methodology of performing BiLSTM-based error correction on the local filters and describes a multi-sensor navigation system. Section 5 describes the simulation setup and configuration. Section 6 performs simulation testing on the proposed algorithm and comparative results based on state-of-the-art systems. Section 7 summarizes the paper.

## III. Related Work

For achieving better robustness and fault tolerance, decentralized systems, for example, federated architecture have become popular in recent years. Conventional federated-based multi-sensor navigation systems often rely on adaptive information allocation factor (IAF) which may not effectively address the challenges arising from inherent variations in sensor accuracy, particularly in diverse environmental conditions. Yue et. al. [5] proposed an IAF to adaptively adjust the covariance matrix of a multi-state constraint Kalman filter (MSCKF) based local filter when an abnormal measurement is detected in GNSS/INS/VO navigation system to eliminate issues of GNSS signal interruption. However, their research showed limitations in performance into the visual performance degradation caused by environmental effects such as lighting variation and motion blur. However, it is essential to consider such fault factors for a comprehensive understanding of the system's performance in the absence of a GNSS signal. As a result, there is a need to explore error correction mechanisms in such systems for uninterrupted flights in GNSS-degraded and denied environments.

The reliance of IAF to correct the error measurements of VIO-based local filter for better accuracy doesn't inherently account for the dynamic of environmental interference such as lighting variations, motion blur, and motion variance. This limitation becomes pronounced when transmitting between environments with varying levels of sensor performance. It is discovered that most of the federated multi-sensor systems used widely preferred fusion algorithms refer to Kalman filters as local filters and master filter. Nevertheless, their intrinsic sensitivity to system dynamics and intricacies of parameter configurations can lead to suboptimal performance, particularly in non-linear and non-Gaussian contexts. In contrast, emerging deep-learning methodologies effectively address these challenges [6], [7]. However, the trade-off involves a substantial dependency on vast datasets and considerable computational capacity. Furthermore, the efficacy of these deep-learning techniques in scenarios diverging from the training domain remains under academic review. However, epistemic uncertainty

can arise due to inherent noise in the sensors and environmental variation while collecting more training data. Techniques such as Bayesian neural networks or Bayesian inferential methodologies, e.g. Monte Carlo dropouts, provide a probabilistic framework to estimate this uncertainty. Addressing epistemic uncertainty can be achieved by enhancing the model's structure, fine-tuning its parameters, or expanding the training dataset. The decrease in this uncertainty enhances the ability of the model to generalize, allowing it to proficiently handle out-of-domain data, which is data not represented in the training sets[8].

Researchers have incorporated machine learning with KF in various ways including compensating errors at the output of KF using machine learning [9]. This integration enables learning-based algorithms to better handle complex scenarios by assessing the level of epistemic uncertainty, adapting to varying sensor conditions and fault patterns. To resolve the inherent non-linearity caused by fault factors present in navigation environments, the paper presents and explores a multi-sensor alternative to GNSS navigation based on a federated architecture with an error detector and machine learning-based error correction. This integration enhances the system's ability against non-gaussian error, mathematical model error and sensor error under diverse fault conditions.

Song et. al [10] has introduced Backpropagation Neural Network (BPNN) in a federated structure for estimating the initial attitude misalignment angle from the master inertial navigation system (MINS) and the velocity and angularity of the slaver inertial navigation system (SINS). Errors that come from the federated Kalman filter (FKF) local filters are corrected using a BPNN and then fused into the master filter. Results show an improvement with respect to conventional FKF, particularly when the dynamic model and noise statistics of INS are ambiguous. Bitar [11] has developed a fusion algorithm that integrates a BPNN with an Unscented Kalman Filter (UKF) at the output of the filter, aiming to diminish tracking errors in distributed acoustic sensor networks. This approach effectively addresses target maneuverability and displays low sensitivity to model parameters. Other similar approaches, like [12] implemented Information Fusion KF with a BPNN for error estimation, which is enhanced with Particle Swarm Optimization (PSO) for the optimization of weights and thresholds. However, supervised learning-based algorithms, such as BPNN, which are better suited for static and non-sequential problems, often overlook the valuable information contained in historical data. Furthermore, navigation applications inherently involve time-dependent and dynamic elements, posing challenges for modeling with these learning algorithms. Given the advantages of having memory capability, less computational complexity and enhanced sequential learning BiLSTM is utilized for the error compensation in this paper.

Other studies have investigated hybrid VIO approaches incorporating CNN-LSTM-based visual odometry to extract essential features for prediction position [7], [13] and updating measurements of Extended Kalman Filter (EKF) [14], [15]. Revach et. al [15] employed GRUs to predict VO position and update EKF measurements. However, such approaches exhibited limited performance due to inadequate datasets replicating complex scenarios. An alternative technique suggested in [16] involves an error corrector for adjusting KF measurements - a solution with a promising performance improvement due to a better resilience to out-of-distribution type of issues often present in test data. Subsequently, leveraging a learning-based error correction mechanism to compensate for the errors of the Kalman filter in order to improve positioning under diverse environments remains an open research area and motivates the work conducted in this study.

#### IV. Proposed Multi-Sensor Navigation System

Considering the need to ensure fault tolerance and reliability of multi-sensor alternative to the GNSS navigation system, the decentralized fusion architecture is adopted in this paper. Figure 1 shows the structure of the multi-sensor hybrid navigation system combining IMU, VO, barometer and GNSS with aiding from an AI-based error correction mechanism.

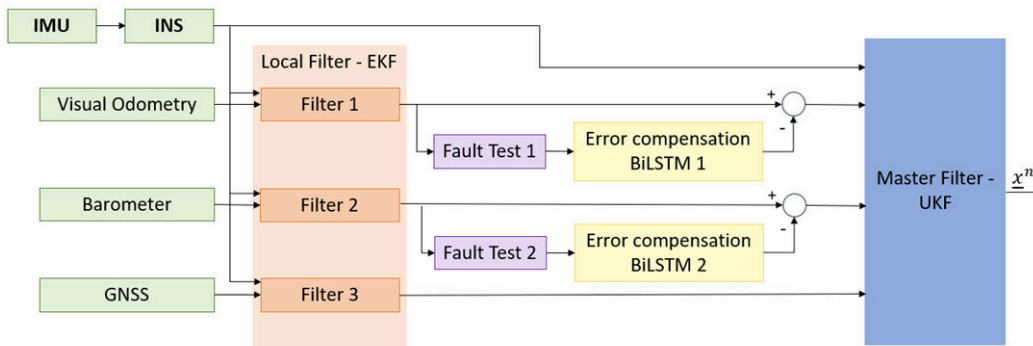


Figure 1. High-level architecture of the proposed solution.

GNSS is included in the system, however, in this study it has intermittent availability. At lower altitudes, the camera field of view restricts the number of features captured. Consequently, GNSS was utilized during both take-off and landing. Specifically, during the take-off, it was crucial to provide initial absolute positioning. The system

employs INS as a contributor to both local filters 1 and 2 which utilize observation information for estimating the 2D position from VO, and the vertical position from the barometer. The preference for EKF as local filters stems from its wide acceptance for this purpose, specific non-ideal behavior while handling nonlinearities, but good computation efficiency and suitability for real-time applications. The filtering results obtained from the local filters are the inputs to the master filter based on UKF. The residual test statistics-based fault detection methodology has been accepted as a switch to activate the error compensation module and optimize in that way computational complexity of the system. This module is configured to remain dormant, with its values below the threshold in the absence of faults. BiLSTM-based error compensator corrects outputs of local filters in the presence of faulty measurements. This comprehensive architecture, combined with the error corrector mechanism, is expected to demonstrate a significant improvement in the performance of an alternative to the GNSS navigation system in challenging scenarios.

### A. Local Filters

In the filtering methods of VIO and barometer/INS integrations, tightly coupled architecture is implemented using EKF. Measured by VO position and INS measurements are utilized to estimate the state vector, as follows-

$$\hat{\mathbf{x}}_k = [x^n, y^n, z^n, v_x^n, v_y^n, v_z^n, a_x^n, a_y^n, a_z^n, \lambda_x, \lambda_y]_k^T$$

Here,  $x^n, y^n, z^n$  denote VIO measured position along x and y axes and barometer/INS measured position along the z-axis;  $v_x^n, v_y^n$  denote VIO measured velocity along x and y axis respectively, while  $v_z^n$  denotes barometer/INS measured velocity along z-axis;  $a_x^n, a_y^n$  stand for VIO measured attitude along x and y axes respectively;  $a_z^n$  denotes barometer/INS measured attitude along z-axis.

Additionally,  $\lambda_x, \lambda_y$  denote scale factors corresponding to VO estimated position at the x and y axes respectively. The estimated scale factors adjust and optimize the accuracy of the VO estimates for a more precise positioning solution.

The widely adopted tightly coupled EKF fusion strategy is employed here based on [17]. The state equations are as follows:

$$\hat{\mathbf{x}}_k^- = f(\hat{\mathbf{x}}_{k-1}, \mathbf{u}_{k-1}) \quad (1)$$

$$\hat{\mathbf{x}}_k^- = F_k \hat{\mathbf{x}}_{k-1} \quad (2)$$

$$P_k^- = F_k P_{k-1} F_k^T + G_k Q_k G_k^T \quad (3)$$

$$\hat{\mathbf{x}}_k = \hat{\mathbf{x}}_k^- + K_k \mathbf{v}_k \quad (4)$$

$$S_k = H_k P_k^- H_k^T + R_k \quad (5)$$

$$P_k = (I - K_k H_k) P_k^- \quad (6)$$

Here,  $\hat{\mathbf{x}}_k^-$ ,  $\hat{\mathbf{x}}_{k-1}$  represent the system state vector at  $k$  and  $k - 1$  epoch;  $P_k^-$ ,  $P_k$  represent the state transition matrix and measurement covariance matrix;  $K_k$  represents Kalman gain;  $H_k$  represents measurement matrix.  $Q_k$ ,  $\mathbf{v}_k$  represent system processing noise and residuals vector. Regarding the measurements, they encompassed only the position variables from each state vector, excluding velocity and acceleration, since only position error was compensated. Finally, only the variables referring to the position in  $\hat{\mathbf{x}}_k^n$  constituted the output of the master filter.

### B. Error Detectors

By analyzing the residual,  $\mathbf{v}_k$ , and the variance of the residual,  $S_k$ , from equations (4) and (5) respectively, of the EKFs, faults can be detected. A test statistic in the residual space was formulated to assess whether the residuals of a particular filter align with their anticipated distribution. For this research, fault detection was conducted from the distribution that emerges when the squared Mahalanobis distances are summed over a series of pre-update residuals, adopted from [18].

The criterion for detecting fault is given by equation (7), where  $(1 - \alpha)$  is the confidence level.

$$\begin{cases} \chi^* > \chi^2(1 - \alpha, M \times Z_i) & \text{Fault} \\ \chi^* \leq \chi^2(1 - \alpha, M \times Z_i) & \text{No fault} \end{cases} \quad (7)$$

From Figure 1, it is observed that the fault detection is different for EKF 1 and EKF 2. Both were set to maintain a confidence level of 95%, along with a number of trailing samples,  $M$ , of 1, as described in [19]. In the first local filter, the dimensionality of  $Z_i$  was set to 4, reflecting the complexity of the residual that encompasses both the horizontal position and the scale factor. Conversely, for the second local filter, where the residual is solely concerned with the vertical position,  $Z_i$  was designated as 1.

### C. Implementation of BiLSTM for Error Correction

As illustrated in Figure 2, the neural network was implemented to estimate the discrepancies between the local filter's output and the true states, enhancing the KF performance. In Figure 2, the inputs and the outputs of the BiLSTM are illustrated without the fault detection module. The inputs are composed of those KF parameters

that directly influence the error: the difference between the state prediction and the previous state estimation,  $\hat{x}_k - \hat{x}_{k|k-1}$ , the difference between the measurement and the observation estimation,  $\hat{z}_k - h(\hat{x}_k)$ , and the positional gain elements of the EKF's gain,  $K_k$  [20]. The BiLSTMs are trained under supervised learning implementing the error between the real position and the model's estimation.

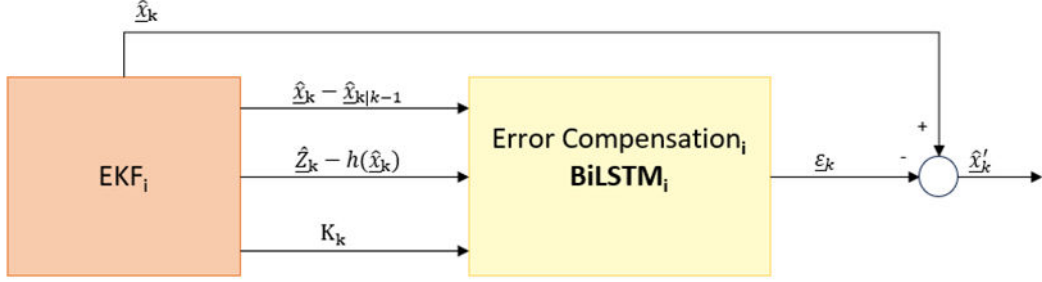


Figure 2. Error compensation structure without fault detection module.

In the local filter 1, VIO, the position is represented by two distinct coordinates,  $x^n$  and  $y^n$ . This requires a decomposition of both inputs and outputs into these respective components. Consequently, instead of three, there are six inputs, with two corresponding outputs, as shown in equation (8). In contrast, local filter 2 only estimates the z-component of the position, thereby requiring three inputs and a single output, as specified in equation (9).

$$\varepsilon_{1k} = [\varepsilon_x, \varepsilon_y]_k \quad (8)$$

$$\varepsilon_{2k} = [\varepsilon_z]_k \quad (9)$$

Regarding the architecture of the neural network, a combination of manual tuning and algorithms such as Random Search was implemented to optimize the hyperparameters. This design was pursued to reduce the epistemic uncertainty outlined previously. Ultimately, the solution that yielded the best results, while controlling overfitting, consisted of a neural network with two BiLSTM layers containing 128 and 32 neurons respectively, and a dropout rate of 0.2. It was complemented with a fully connected layer with 50 neurons and followed by the output layer.

#### D. Master Filter

For the master filter, a UKF was selected due to its improved performance when working with nonlinearities. Mathematical description of the UKF is summarized in Table 1.

Table 1. Algorithm description of the UKF.

##### Inputs

$\underline{x}_{k-1|k-1}^a, P_{k-1|k-1}^a$ , priori estimated state and covariance matrix.  
 $u_{k-1}$ , control input  
 $Q_k, R_k$ , process and measurement noise covariance matrices

##### Outputs

$\hat{x}_{k|k}, P_{k|k}$ , posterior estimated state and covariance matrix

**Step 1:** Prediction at time  $k$  with the Unscented Transform.

$$X_{k-1|k-1}^0 = \underline{x}_{k-1|k-1}^a \quad (10)$$

$$X_{k-1|k-1}^i = \underline{x}_{k-1|k-1}^a + \left( \sqrt{(L + \lambda) P_{k-1|k-1}^a} \right)_i, i = 1, \dots, L \quad (11)$$

$$X_{k-1|k-1}^i = \underline{x}_{k-1|k-1}^a - \left( \sqrt{(L + \lambda) P_{k-1|k-1}^a} \right)_i, i = (L + 1), \dots, 2L \quad (12)$$

$$\lambda = \alpha^2(L + k) - L \quad (13)$$

Where  $k = 3 - N$ , being  $N$  the number of states.

The sigma points are propagated through the nonlinear function  $f(\cdot)$ .

$$X_{k-1|k-1}^i = f(X_{k-1|k-1}^i), \quad i = 0, \dots, 2L \quad (14)$$

To calculate the predicted state and covariance of the approximate Gaussian, the sigma points are weighted.

$$\hat{x}_{k|k-1}^a = \sum_{i=0}^{2L} W_s^i X_{k-1|k-1}^i \quad (15)$$

$$P_{k|k-1} = \sum_{i=0}^{2L} W_c^i [X_{k-1|k-1}^i - \hat{x}_{k|k-1}^a][X_{k-1|k-1}^i - \hat{x}_{k|k-1}^a]^T + Q_k \quad (16)$$

$$W_s^0 = \frac{\lambda}{L + \lambda}, \quad W_c^0 = \frac{\lambda}{L + \lambda} + (1 - \alpha^2 + \beta) \quad (17)$$

$$W_s^i = W_c^i = \frac{\lambda}{2(L + \lambda)} \quad (18)$$

**Step 2:** Corrected prediction at time  $k$  given the measurement model.

The noise-augmented state of the measurement is calculated with the equations (10), (11), and (12). The sigma points are propagated through the nonlinear function  $h(\cdot)$ .

$$\gamma_k^i = h(X_{k-1|k-1}^i), \quad i = 0, \dots, 2L \quad (19)$$

$$\hat{z}_k = \sum_{i=0}^{2L} W_s^i \gamma_k^i \quad (20)$$

$$P_{k|k-1} = \sum_{i=0}^{2L} W_c^i [\gamma_k^i - \hat{z}_k][\gamma_k^i - \hat{z}_k]^T + R_k \quad (21)$$

Then the state-measurement cross-covariance matrix is calculated to compute the UKF Kalman gain.

$$P_{x_k z_k} = \sum_{i=0}^{2L} W_c^i [X_{k-1|k-1}^i - \hat{x}_{k|k-1}^a][\gamma_k^i - \hat{z}_k]^T \quad (22)$$

$$K_k = P_{x_k z_k} P_{z_k z_k}^{-1} \quad (23)$$

State estimate and error covariance are updated

$$\hat{x}_{k|k} = \hat{x}_{k|k-1} + K_k (\underline{z}_k - \hat{z}_k) \quad (24)$$

$$P_{k|k} = P_{k|k-1} - K_k P_{z_k z_k} K_k^T \quad (25)$$

## V. Simulation Environment

To validate the proposed solution, the Hardware in the Loop (HIL) configuration depicted in Figure 3 was established. This simulation environment was part of the setup implemented in [21]. A Pixhawk 2.4 board was used as the primary Flight Control Unit (FCU) for the navigation and control of the UAS. This was directly connected to a local computer, which served as the Companion Computer (CC) in which monocular camera data was processed. To simulate real environments and sensor measurements, Unreal Engine and Cesium are incorporated along with AirSim to connect the FCU directly to the environment generation framework. The trajectory commands were produced within a Python script directly linked to AirSim. A high level of detail in the environment was achieved through the integration of photogrammetry data exported from Google Earth within the Unreal Engine. For the scope of this work, the simulation of Toulouse, depicted in Figure 4, was implemented.



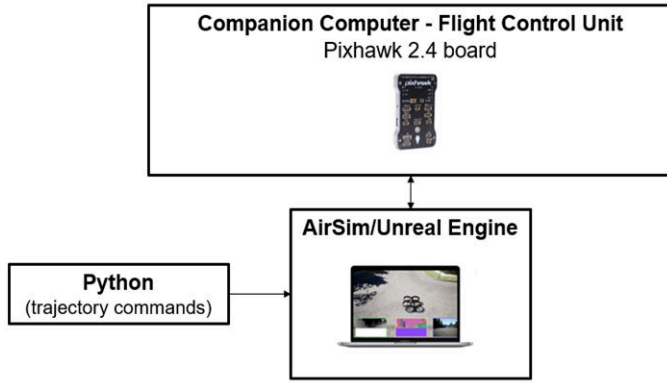


Figure 3. Hardware in the Loop setup.



Figure 4. Toulouse 3D simulation.

The IMU sensor specification is shown in Table 2.

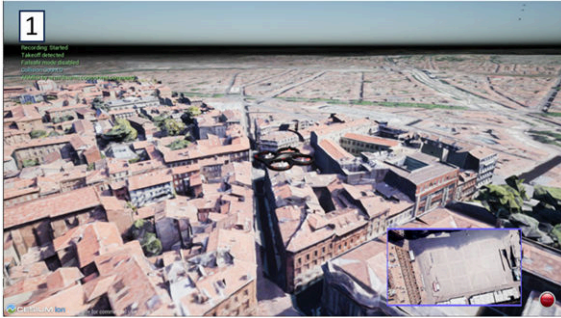
Table 2. IMU sensor configuration.

	Gyroscope	Accelerometer
Bias	$2.85e-5$ rad/s	$1e-5$ m/s <sup>2</sup>
Random walk	$1.2e-6$ (rad/s)/ $\sqrt{s}$	$1.2e-6$ (m/s <sup>2</sup> )/ $\sqrt{s}$

## VI. Performance Evaluation

### A. Simulation Results

One of the significant drawbacks of the visual navigation system is its high sensitivity to environmental conditions, such as rain or snow, and to changes in lighting. Thus, to validate the alternative to GNSS navigation system performance, the research focuses on the impact of these changes on horizontal positioning. In order to evaluate the performance of the proposed approach with the error correction mechanism, the simulations were executed under conditions emulating the midday solar illumination characteristic of the scene. In this research, four different scenarios are considered: 20% fog intensity, 100% rainfall, 80% snow (illustrated in Figure 5), and evening light conditions with reduced luminosity and strong building shadows as depicted in Figure 6. Figure 5(4) illustrates the flight trajectory covering a distance of 400m at an altitude of 70m that has been selected for testing in the simulated environment incorporating an error correction mechanism.



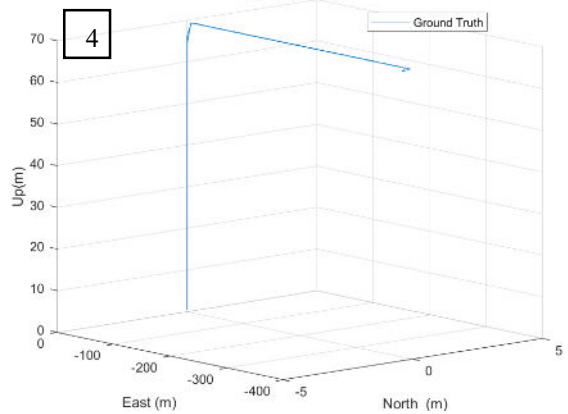
1) 100% Rain



2) 80% Snow



3) 20% Fog



4) Flight trajectory

Figure 5. Simulation environment featuring the experimental path

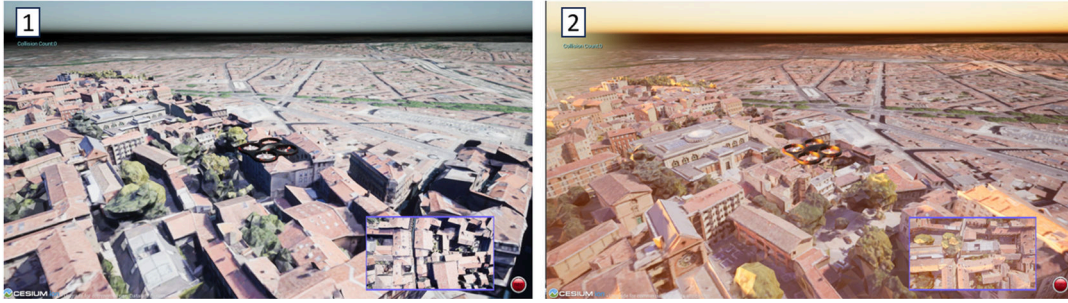


Figure 6. Simulation environment with 1) Midday light 2) Evening light.

Training and testing datasets are selected from the simulated environment generated by multiple complex scenarios incorporating various trajectories. For training 12 trajectories were employed, featuring straight lines of varying lengths at 70 m of altitude. These trajectories had changing x-y coordinates and spanned approximately 200 m - 800 m in length, resulting in the inclusion of over 500,000 samples from each sensor. Training datasets replicate the fault conditions and environmental conditions including high-altitude flights, low-altitude flights, snow, rain, dust, sunny, partly sunny, dusk, fog, motion blur and UAV dynamics. Three data sources from EKF measurements such as position increments, innovation and Kalman gain are generated and used to train the BiLSTM module for each trajectory. In the testing phase, upon fault detection, BiLSTM-based error correction scheme predicts the corrected position increment which is then updated with EKF measurement and fed as input to the UKF module. Additionally, since the model was trained on trajectories at an altitude of 70 m, it is not able to generalize and predict a greater error with the altitude increase. A viable approach to address this limitation might be to train the model across various altitudes.

## B. Positioning Performance

In Figure 7 and Figure 8, the outcomes of the VO are presented, illustrating how the problem of the scale factor is addressed through the use of VIO. Comparing the different graphs, it is observed that rain, snow, or fog, even different light intensities, cause a higher divergence of the VO compared to midday lighting conditions, especially along the North coordinate. For example, even with low intensities of fog, the VO estimates position is far from its corresponding location at the end of the simulation. In the case of the evening lightning, the primary source of error of the VO is found along the East coordinate.

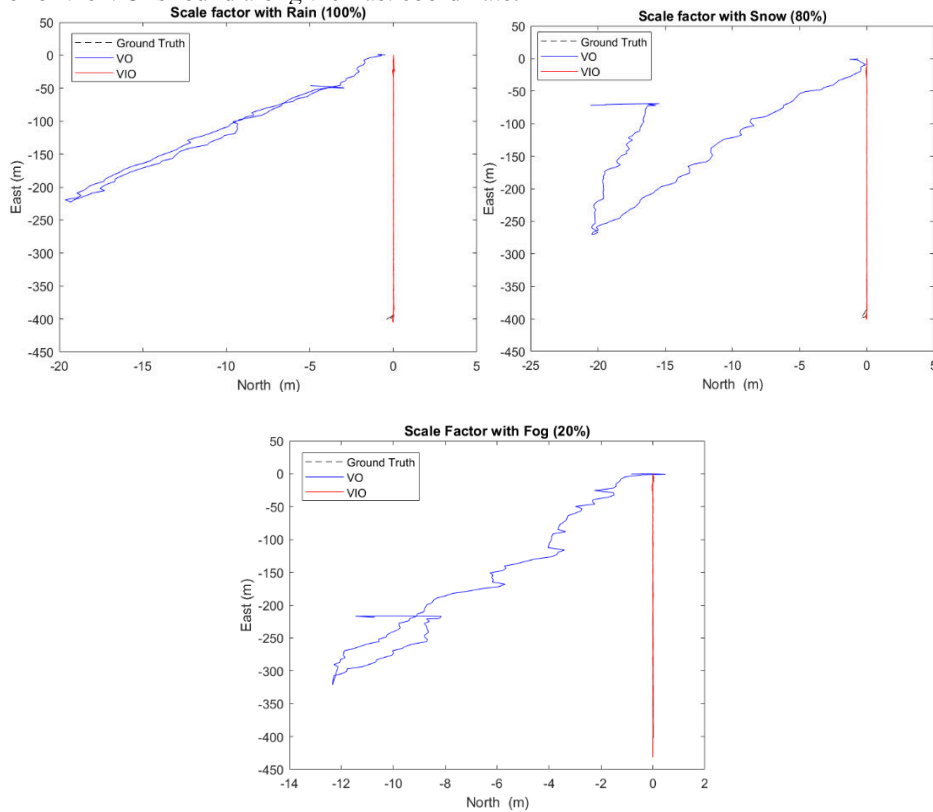


Figure 7. Scale factor with different environmental conditions.



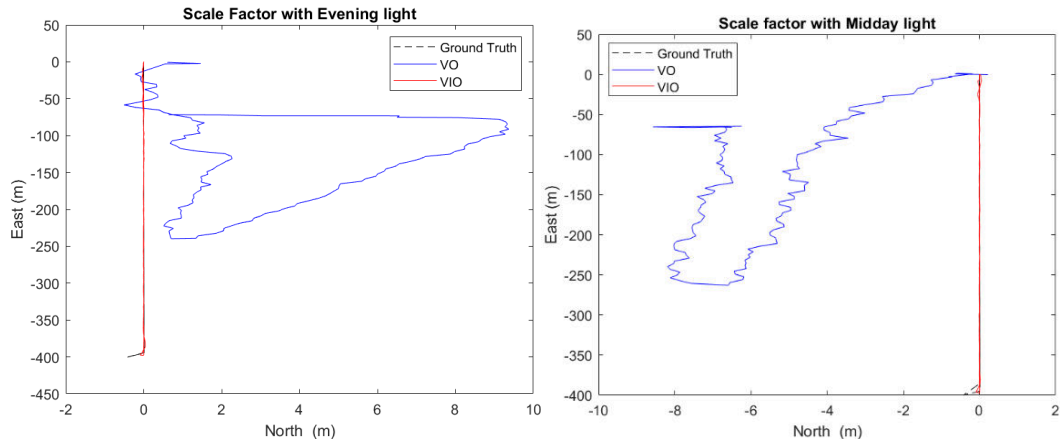


Figure 8. Scale factor with different lighting conditions.

The results of the master filter with error compensation are displayed in Figure 9. The term 'normal' was used here to refer to the environmental condition where the solar time is corresponding to the midday, and the weather is sunny.

A significant increase in position error is observed in Figure 9 under foggy conditions. The primary source of this error is because of the feature-matching algorithm and it is resulting in feature tracking error, feature extraction error and feature association error. When altering the field of view of the camera with the fog, the VO algorithm matches fewer features between frames, resulting in a deterioration of the outcome. In the case of rain and snow, even for their elevated intensities, the outcome is only marginally inferior to normal conditions. Such effects introduce particles into the field of vision, negatively affecting the result, and particularly hindering the performance of the feature-matching algorithm. However, if these particles move sufficiently fast, their impact on the availability and traceability of the features is less pronounced. Thus, while the result does degrade, it is not as markedly affected as it is by fog.

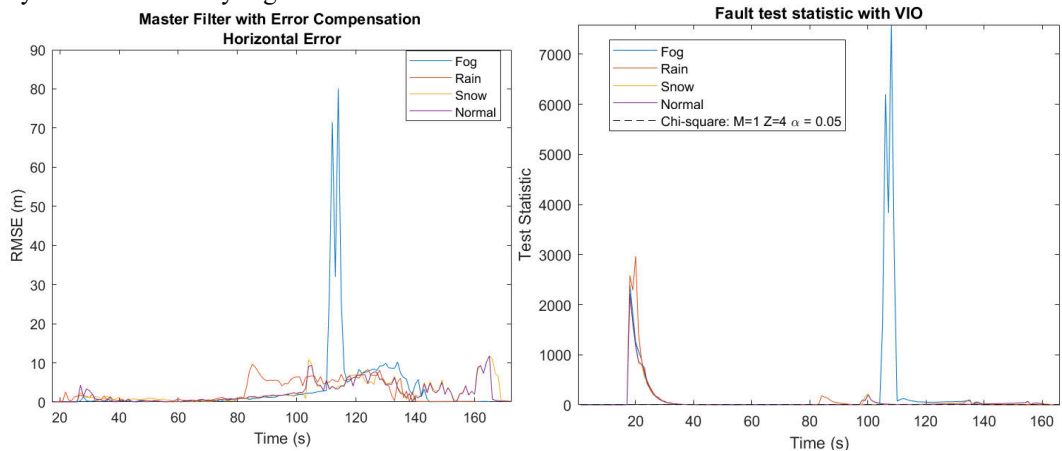


Figure 9. Results Outputs of the master filter with error compensation with different weather conditions. On the left: horizontal RMSE. On the right: fault test statistics for VIO.

The observed behavior of the system is summarized in Table 3. Under snow conditions, error compensation results in a 42% reduction in RMSE, while in rainy conditions, the reduction is 34%. This discrepancy is attributable to the fact that in the case of rain, the error at the end of the first segment of the trajectory is not detected as a failure and therefore it is not compensated. In the case of fog, the error reduction by the proposed compensation mechanism is 20%. In this scenario, the error is significantly different from the models implemented for training, leading to inferior results.

Table 3. Comparison of the horizontal position error of the master filter with error compensation with different weather conditions.

	Rain 100%	Snow 80%	Fog 20%	Normal conditions
<b>Master Filter w/o Error Compensation</b>	4.39 m	4.41 m	5.11 m	4.33 m

<b>Master Filter with Error Compensation</b>	2.91 m	2.55 m	4.05 m	2.43 m
--	--------	--------	--------	--------

One can see from Figure 10 that at lower light conditions the overall error is higher. This increase is attributed to a reduction in the number of features to detect, causing the VO algorithm to yield inferior results. Consequently, the performance of the entire system is compromised. Additionally, at the end of the simulation, the VO becomes unavailable at the earlier stage in the evening lighting case.

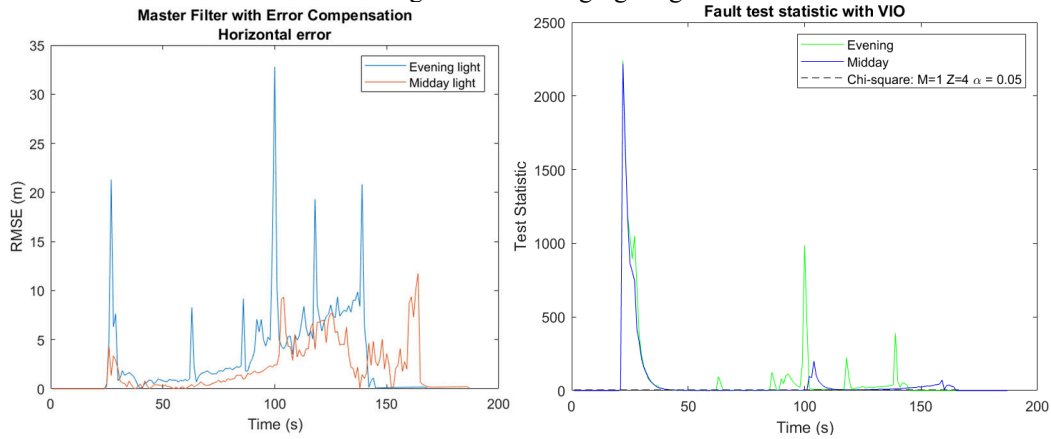


Figure 10. Results for the master filter with error compensation with different lighting conditions. On the left: horizontal RMSE. On the right: fault test statistics for VIO.

Table 4 summarizes the observed error in this case, emphasizing that under normal lighting conditions, the error compensation mechanism is introducing a 44% reduction in the position error. However, in the evening lighting scenario, the improvement is limited to 15%. It has been also noted on a number of occasions that the efficiency of error compensation declines when applied to out-of-domain data.

Table 4. Comparison of the horizontal mean RMSE of the master filter with error compensation with different lighting conditions.

	<b>Evening light conditions</b>	<b>Daylight conditions</b>
<b>Master Filter w/o Error Compensation</b>	5.13 m	4.33 m
<b>Master Filter with Error Compensation</b>	4.34 m	2.43 m

### C. Analysis and Discussion

The study presented in [21] was selected for comparative analysis due to its use of the same VO and a similar simulation framework. In that study, a federated architecture is employed too, but with a GRU as the master filter. The objective is to incorporate INS and VO to enhance the navigation performance degraded by GNSS outages, but GNSS is considered to be generally available for the whole duration of the simulation. Moreover, INS drift is corrected with another GRU before the fusion within the local filters.

Table 5 presents the results from VIO and the output of the master filter from both works. For a better understanding, results from [21] with and without the INS correction by GRU are provided. In this case, the values corresponding to the trajectory are used for comparison, as both trajectories have similar lengths.

Table 5. Horizontal mean RMSE of VIO and master filter obtained in [21] and in the present work.

	<b>VIO (without INS GRU aid) [21]</b>	<b>VIO (with INS GRU aid) [21]</b>	<b>Present work</b>
<b>VIO Local Filter</b>	7.31 m	4.26 m	4.42 m
<b>Master Filter</b>	1.08 m	0.80 m	2.43 m

A higher value of the VIO error from [21] without INS correction by GRU is attributed to the presence of uncompensated IMU bias and random walk. The quality of the IMU implemented in [21] is lower than the IMU implemented in the present work, but with the INS-GRU scheme, similar values to the present work are obtained.

Finally, results from the master filter show that even without the implementation of the GRU aid to the INS, the performance of [21] exceeds that in the present works, which can be attributed to the presence of GNSS over a significant part of the simulation. An additional factor is the implementation of the GRU as the master filter which is believed to be a strong competitor to the UKF with the BiLSTM error compensation proposed in this study.

## VII. Conclusion

Ensuring the accuracy and integrity of autonomous vehicle navigation systems in GNSS-denied environments is of paramount significance. To complement the widely adopted aiding sensor IMU and reduce its inherent long-term drift, this study adopted federated multi-sensor fusion architecture incorporating a camera and barometer to aid 3D positioning of the UAS in GNSS-denied environments. Within this framework, residual test statistics-based fault detection modules after the local filters are included. To mitigate the effects of measurement faults and increase robustness under diverse environmental fault conditions, the errors from the outputs of the local filters are compensated using the proposed BiLSTM-based error corrector before fusion in the master filter.

The main advantages of using BiLSTM-based error correction within the federated multi-sensor navigation system are as follows: (1) BiLSTM excels in capturing temporal dependency in sequential data, reducing overfitting issues and consider not to introduce significant latency compared to other machine learning models, 2) the learning-based correction is able to effectively capture nonlinearity and fault patterns available in training dataset. Thus, the proposed alternative to GNSS multi-sensor navigation system possesses superior accuracy and robustness, particularly in complex weather conditions including 44% in rain, 20% in snow and lighting conditions covering 15% during evening and 44% during daylight.

However, the error compensation is sensitive to the training data used, making epistemic uncertainty still noticeable even after correction applied. It is also difficult for the model to generalize the error among the variety of trajectories due to VO performance variability. The proposed approach incorporating error correction represents a step forward in improving the robustness and reliability of vision-based alternative to GNSS system, particularly in complex and dynamic environments where feature extraction error and feature association error are critical for accurate navigation.

Future work planned will focus on a comprehensive study to evaluate the performance and generalization ability of learning-based of error compensation techniques for Kalman filter-based architectures aiming to achieve improved positioning accuracy and robustness.

## Acknowledgments

The authors thank Boeing UK for the contribution to this study, in particular, information on the problem space and the challenges, which helped to shape the solution and evaluation scheme.

## References

- [1] C. Campos, R. Elvira, J. J. G. Rodriguez, J. M. M. Montiel, and J. D. Tardos, "ORB-SLAM3: An Accurate Open-Source Library for Visual, Visual-Inertial, and Multimap SLAM," *IEEE Transactions on Robotics*, vol. 37, no. 6, pp. 1874–1890, Dec. 2021, doi: 10.1109/TRO.2021.3075644.
- [2] T. Qin, P. Li, and S. Shen, "VINS-Mono: A Robust and Versatile Monocular Visual-Inertial State Estimator," Aug. 2017, doi: 10.1109/TRO.2018.2853729.
- [3] P. Geneva, K. Eickenhoff, W. Lee, Y. Yang, and G. Huang, "OpenVINS: A Research Platform for Visual-Inertial Estimation," *Proc IEEE Int Conf Robot Autom*, pp. 4666–4672, May 2020, doi: 10.1109/ICRA40945.2020.9196524.
- [4] F. Ma, J. Shi, Y. Yang, J. Li, and K. Dai, "ACK-MSCKF: Tightly-coupled ackermann multi-state constraint kalman filter for autonomous vehicle localization," *Sensors (Switzerland)*, vol. 19, no. 21, Nov. 2019, doi: 10.3390/s19214816.
- [5] J. Dai, X. Hao, S. Liu, and Z. Ren, "Research on UAV Robust Adaptive Positioning Algorithm Based on IMU/GNSS/VO in Complex Scenes," *Sensors (Basel)*, vol. 22, no. 8, Apr. 2022, doi: 10.3390/S22082832.
- [6] B. Wagstaff, E. Wise, and J. Kelly, "A Self-Supervised, Differentiable Kalman Filter for Uncertainty-Aware Visual-Inertial Odometry," *IEEE/ASME International Conference on Advanced Intelligent Mechatronics, AIM*, vol. 2022-July, pp. 1388–1395, 2022, doi: 10.1109/AIM52237.2022.9863270.
- [7] M. F. Aslan, A. Durdu, and K. Sabanci, "Visual-Inertial Image-Odometry Network (VIIONet): A Gaussian process regression-based deep architecture proposal for UAV pose estimation," *Measurement*, vol. 194, p. 111030, May 2022, doi: 10.1016/J.MEASUREMENT.2022.111030.
- [8] R. L. Russell and C. Reale, "Multivariate Uncertainty in Deep Learning," *IEEE Trans Neural Netw Learn Syst*, vol. 33, no. 12, pp. 7937–7943, Dec. 2022, doi: 10.1109/TNNLS.2021.3086757.

- [9] S. Kim, I. Petrunin, and H. S. Shin, "A Review of Kalman Filter with Artificial Intelligence Techniques," in *Integrated Communications, Navigation and Surveillance Conference, ICNS*, Institute of Electrical and Electronics Engineers Inc., 2022. doi: 10.1109/ICNS54818.2022.9771520.
- [10] L. Song, Z. Duan, B. He, and Z. Li, "Application of Federal Kalman Filter with Neural Networks in the Velocity and Attitude Matching of Transfer Alignment," *Complexity*, vol. 2018, 2018, doi: 10.1155/2018/3039061.
- [11] N. Al Bitar and A. I. Gavrilov, "Neural Networks Aided Unscented Kalman Filter for Integrated INS/GNSS Systems," *27th Saint Petersburg International Conference on Integrated Navigation Systems, ICINS 2020 - Proceedings*, May 2020, doi: 10.23919/ICINS43215.2020.9133878.
- [12] Y.-H. Yang and Y. Shi, "Application of Improved BP Neural Network in Information Fusion Kalman Filter," *Circuits Syst Signal Process*, vol. 39, pp. 4890–4902, 2020, doi: 10.1007/s00034-020-01393-y.
- [13] C. Li and S. L. Waslander, "Towards End-to-end Learning of Visual Inertial Odometry with an EKF," *Proceedings - 2020 17th Conference on Computer and Robot Vision, CRV 2020*, pp. 190–197, May 2020, doi: 10.1109/CRV50864.2020.00033.
- [14] B. Wagstaff, E. Wise, and J. Kelly, "A Self-Supervised, Differentiable Kalman Filter for Uncertainty-Aware Visual-Inertial Odometry," *IEEE/ASME International Conference on Advanced Intelligent Mechatronics, AIM*, vol. 2022-July, pp. 1388–1395, 2022, doi: 10.1109/AIM52237.2022.9863270.
- [15] G. Revach, N. Shlezinger, X. Ni, A. L. Escoriza, R. J. G. Van Sloun, and Y. C. Eldar, "KalmanNet: Neural Network Aided Kalman Filtering for Partially Known Dynamics," *IEEE Transactions on Signal Processing*, vol. 70, pp. 1532–1547, 2022, doi: 10.1109/TSP.2022.3158588.
- [16] S. Kim, I. Petrunin, and H. S. Shin, "A Review of Kalman Filter with Artificial Intelligence Techniques," *Integrated Communications, Navigation and Surveillance Conference, ICNS*, vol. 2022-April, 2022, doi: 10.1109/ICNS54818.2022.9771520.
- [17] X. Xiong, W. Chen, Z. Liu, and Q. Shen, "DS-VIO: Robust and Efficient Stereo Visual Inertial Odometry based on Dual Stage EKF," May 2019, [Online]. Available: <http://arxiv.org/abs/1905.00684>
- [18] J. Jurado, J. Raquet, C. M. Schubert Kabban, and J. Gipson, "Residual-based multi-filter methodology for all-source fault detection, exclusion, and performance monitoring," *Navigation*, vol. 67, no. 3, pp. 493–510, Sep. 2020, doi: 10.1002/NAVI.384.
- [19] J. H. Choi, Y. W. Park, J. Kim, T. S. Choe, and J. B. Song, "Federated-filter-based unmanned ground vehicle localization using 3D range registration with digital elevation model in outdoor environments," *J Field Robot*, vol. 29, no. 2, pp. 298–314, Mar. 2012, doi: 10.1002/ROB.21416.
- [20] Z.-J. Yu, S.-L. Dong, J.-M. Wei, T. Xing, and H.-T. Liu, "Neural Network Aided Unscented Kalman Filter for Maneuvering Target Tracking in Distributed Acoustic Sensor Networks," 2007.
- [21] S. A. Negru, P. Geragersian, I. Petrunin, A. Zolotas, and R. Grech, "GNSS/INS/VO fusion using Gated Recurrent Unit in GNSS denied environments," Jan. 2023, doi: 10.2514/6.2023-2226.

2024-01-04

# Hybrid multi-sensor navigation system with uncertainty correction for GNSS-denied environments

Villalonga Torres, Mar

AIAA

---

Villalonga Torres M, Elmi Tabassum T, Petrunin I, Tsourdos A. (2024) Hybrid multi-sensor navigation system with uncertainty correction for GNSS-denied environments. In: AIAA SCITECH 2024 Forum, 8-12 January 2024, Orlando, USA. Paper number AIAA 2024-2799  
<https://doi.org/10.2514/6.2024-2799>

*Downloaded from Cranfield Library Services E-Repository*